Electronic Supplementary Material (ESI) for Materials Advances.
This journal is © The Royal Society of Chemistry 2020

Supporting Information

Iron-based energy storage materials from carbon dioxide and scrap metal

Joyce S Yeoh,[a] *Iolanda Di Bernardo,*[b,c] *Nicholas G. White,*[d] *Vincent Otieno-Alego,*[e] *Takuya Tsuzuki* [a] *and Adrian Lowe* [a]*

*Corresponding Author: adrian.lowe@anu.edu.au , +61 2 6125 4881

[a]Research School of Electrical, Energy and Materials Engineering, The Australian National University, Canberra, ACT 2601, Australia

[b]School of Physics and Astronomy, Monash University, Clayton, VIC, Australia.

[c]ARC Centre for Future Low Energy Electronics Technologies, Monash University, Clayton, VIC, Australia.

[d]Research School of Chemistry, The Australian National University, Canberra, ACT 2601, Australia

[e]Specialist Operations, Australian Federal Police, Canberra, ACT, 2609

KEYWORDS: Carbon dioxide utilization; waste; iron oxalate; iron oxide; lithium-ion battery; anode materials; electrochemical properties

The supporting information document consists of 24 pages, 12 tables, and 11 figures

Materials and methods

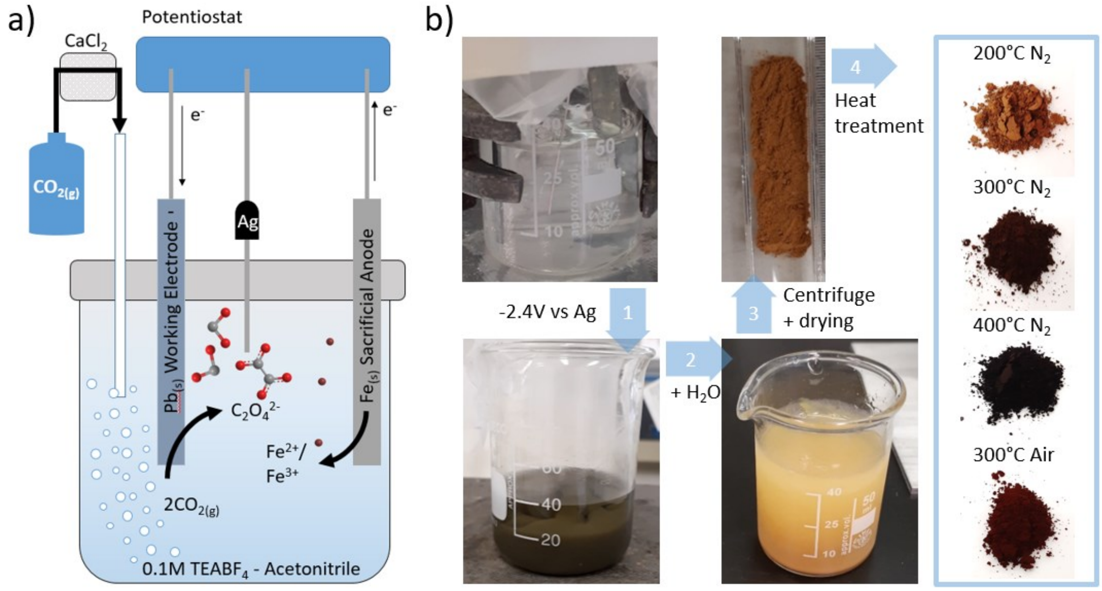

Figure S 1: a) Schematic of the experimental setup used for electrochemical reduction of CO_2 and b) the observed changes to colour and state of products during electrochemical reduction, product isolation and post treatment.

Electrolyte preparation:

Acetonitrile (ACN, 99.8% Anhydrous Sigma Aldrich, 99.5% Ajax Finechem) was dried over 3Å molecular sieves (beads 4 – 8 mesh, Sigma Aldrich) for at least three days before using. The electrolyte salt (99%, Tetraethylammonium tetrafluoroborate, $TEA.BF_4$, Alfa Aesar) was dried in a vacuum oven (NEYTECH Qex) at 80°C for 18 hours before usage. The appropriate amount of salt was dissolved in dried ACN to form a 0.1 M electrolyte solution. The solution was stored with 3Å molecular sieves.

Working electrode preparation (Pb electrode activation)

Before the main electrochemical reduction experiment, the Pb working electrode was activated in 0.1 M $TEABF_4$-ACN solution by applying a potential of -3.0 V vs Ag for 3 minutes. The working electrode was then sonicated in the same batch of electrolyte for 1 minute and rinsed with dry acetonitrile before being inserted into the main electrochemical reduction cell. The electrode was immersed in acetonitrile with 3Å molecular sieves during storage.

Sacrificial electrode preparation

Scrap mild steel was obtained from a scrapyard. Elemental analysis via EDS on SEM was used to verify the composition of the metal. The sheet was cut into electrodes (5 x 15 x 3 mm), rust was removed from the surface using sandpaper (FlexOvit grade P80, P180, P600), followed by ultra-sonication in absolute ethanol for 5 minutes. The electrode was removed, wiped dry with a piece of Kimwipe™ then dried in the drying oven (60°C in air, 10 minutes). The dry electrode was then sonicated in dry acetonitrile (5 minutes), followed by immersion in dry acetonitrile with 3Å molecular sieves for storage.

Electrochemical reduction

Carbon dioxide (CO_2, BOC, Food Grade, UN1013) was bubbled through 100 mL of electrolyte for 30 minutes. After which, 40 ml was transferred into a clean and dry 50 ml glass beaker, with care taken to minimise aerating the electrolyte. The electrodes (Ag wire as a quasi-reference electrode, activated Pb as working electrode, Zn or Fe as counter/sacrificial electrode) were inserted into the template, into the electrolyte, puncturing the cling wrap in the process. A potential of -2.4 V vs Ag was applied using a potentiostat (VMP3 Biologic). The amount of charge delivered during electrochemical reduction was monitored, approximately 250 C and 1250 C were delivered when 40 ml and 200 ml of electrolyte were used, respectively, with slight variations depending CO_2 supply. During the electrochemical reduction process, CO_2 was bubbled through the solution continuously. In all cases, CO_2 was passed through calcium chloride before being bubbled through the electrolyte using a polyethylene tubing (Inner and outer diameter of 2 and 4 mm). The immersed surface area of the working electrode (Pb) was 2 and 6 cm^2 for 40 and 200 ml of electrolyte, respectively.

Product Isolation

Electrodes were removed, and deionised water (40 ml) was gradually added to the electrolyte/product mixture while sonicating the mixture. The solid product was isolated by adding deionised water (equal in volume to the electrolyte) and sonicating the reaction mixture, followed by centrifuging (3 repeating cycles of 3500 rpm for 3 minutes). The liquid portion was decanted after each cycle, and 5 – 10 ml of deionised water added to the residue before the next cycle. The remaining solid was dried at 60°C for at least 16 hours.

Heat Treatment

Heat treatment of the isolated iron compound was performed in a tube furnace (SKGL-1200). Samples (0.7 g per batch) were placed in a quartz boat and inserted into the quartz tube. Heat treatment was performed under N_2 (flow rate of 200 cm^3 min^{-1}) at 200°C, 300°C and 400°C for 2 hours, with a heating rate of 20 °C min^{-1}. The furnace was allowed to cool naturally with continued N_2 flow until the furnace temperature was no greater than 40 °C. Heat treatment in air at 300 °C was performed using a muffle furnace (SEM Muffle Furnace 102C). Heating rates of 20 °C min^{-1} and 3 °C min^{-1} were used for the tube furnace and muffle furnace respectively. Temperatures mentioned were held for 2 hours and the furnace allowed to cool naturally.

Yield calculations

Table S 1: $FeC_2O_4.2H_2O$ Yield Calculations.

Experiment	**Electrolyte Volume [ml]**	**Charge Delivered [C, Coulombs]**	**Product Mass (after drying) [mg]**	**Theoretical yield based [mg]**	**%Yield**
1	40	120	80	112	71
2	40	255	200	238	84
3	40	250	100	233	43
4	40	250	180	233	77
5	40	272.3	192	254	76
6	40	242	193	226	86
7	40	250	157	233	67
8	40	250	167	233	72
9	40	250	210	233	90
10	40	300	209	280	75
11	40	250	164	233	70
12	40	226	151	211	72
13	200	1250	733	1165	63
14	200	1064	633	992	64
15	200	1127	810	1051	77
16	200	1007	706	939	75
17	200	1378	959	1285	75
18	200	18245	1307	1701	77
				Average Yield	73

Since CO_2 and the Fe were provided in excess, yield calculations were based on the charge delivered during electrochemical reduction.

Based on the reaction equation (Eq. S1), two electrons are required in the formation of one oxalate anion.

$$2CO_2 + 2e^- \rightarrow C_2O_4^{2-} \text{ (Eq. S1)}$$

Simultaneously, Iron oxidises and the overall reaction can be summarised by the following equation:

$$Fe + 2CO_2 + 2H_2O \rightarrow FeC_2O_4.2H_2O \text{ (Eq. S2)}$$

The number of moles of electrons in 1 C of charge is given by:

$$n(e^-) = \left(\frac{1}{1.6 \times 10^{-19}}\right) \Big/ N_A \quad \text{(Eq. S3)}$$

Where N_A is Avogadro's number, and one electron has a charge of $1.6 \text{X} 10^{-19}$ Coulombs.

The number of moles of $C_2O_4^{2-}$ and hence $FeC_2O_4.2H_2O$ expected is therefore determined as follows:

$$n\left(C_2O^{2-}_4\right) = n\left(FeC_2O_4.2H_2O\right) = \frac{n\left(e^-\right)}{2} \quad \text{(Eq. S4)}$$

Theoretical mass of product isolated after electrochemical reduction is, therefore:

$$m\left(FeC_2O_4.2H_2O\right) = MW\left(FeC_2O_4.2H_2O\right) \times \frac{n\left(e^-\right)}{2} \quad \text{(Eq. S5)}$$

The molecular weight of $FeC_2O_4.2H_2O$ (MW) is 179.9 g mol^{-1}.

For 100C of charge delivered, 93.2 mg of $FeC_2O_4.2H_2O$ is expected.

The yield was determined as follows:

$$Experimental\ yield = \frac{mass\ of\ product\ isolated}{mass\ of\ product\ expected\ based\ on\ applied\ charge} \quad \text{(Eq. S6)}$$

FTIR and Raman peak assignments for as-isolated $FeC_2O_4.2H_2O$

Features on the FTIR and Raman spectra were assigned to the vibrations of functional groups present in $FeC_2O_4.2H_2O$; FTIR bands between 1600 – 1300 cm^{-1} and the Raman peak between 1470 – 1490 cm^{-1} are attributed to stretching of C-O bonds in the oxalate anions, and the broad FTIR band at 3300 cm^{-1} corresponds to stretching of the O-H bond in H_2O. Further peak assignments are provided in Table S2.

Table S 2: Assignment of the bands in the vibrational spectra (FTIR and Raman) of $FeC_2O_4.2H_2O$ prepared via electro reduction of CO_2 with Fe sacrificial anode. Band intensities are also indicated (vs, very strong; s, strong; m, medium; w, weak; br, broad; sh, shoulder).

IR Peak (cm^{-1})	Raman Peak (cm^{-1})	Assignment
3337 a, br		ν(O-H) (H_2O)
1646, 1621 vs		ν(C-O)
	1470-4790 vs	ν(C-O)
1362 s, 1318 vs		ν (C-O)
	913 s	ν(C-C)
818 m		δ(O-C-O) + ν(C-C)
712 w,br		ρ(H_2O)
530 s/sh	580/523 m	δring
462 s		ν(Fe-O)?

Peak assignments are based on previous publications[1] and general characteristic frequencies of functional groups.

Synthesis and characterisation of $ZnC_2O_4.2H_2O$

The electrochemical synthesis of the oxalate anion from carbon dioxide was verified using NMR spectroscopy on Zinc oxalate dihydrate ($ZnC_2O_4.2H_2O$). NMR analysis is unsuitable for $FeC_2O_4.2H_2O$, as iron oxalates are paramagnetic. In addition to its suitability for NMR analysis, the synthesis of $ZnC_2O_4.2H_2O$ from CO_2 and Zn was previously reported,[2] and its formation can occur at the same applied potential (-2.4 V vs $Ag_{(s)}$) since zinc can oxidise more readily than iron (standard reduction potentials, E°, for Zn and Fe are –0.76 and –0.44 V, respectively). Zinc oxalate dihydrate ($ZnC_2O_4.2H_2O$) was prepared and characterised to verify the synthesis of the oxalate anion from carbon dioxide.

The size of the working electrode influenced the products synthesised, with larger surface areas favouring the formation of cyano complexes (see PXRD in **Figure S 2**).

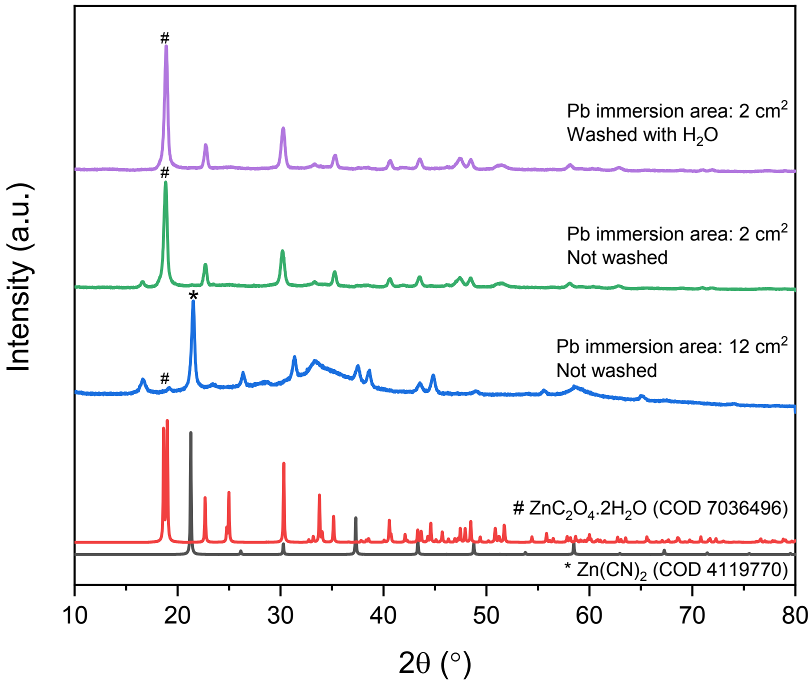

Figure S 2 : PXRD of solid products isolated after electroreduction was performed in 40 ml of electrolyte using two different surface areas of Pb (12 cm^2 and 2 cm^2). Electrolysis was performed at -2.4 V vs Ag. The diffraction peak at 16.5° disappears after the product is washed with H_2O.

NMR spectra were collected on a Bruker Avance 400 spectrometer and referenced to 1,4-dioxane.[3] The samples were prepared by dissolving synthesised zinc oxalate dihydrate in D_2O containing DCl, and 1,4-dioxane as an internal standard, forming a solution containing $ZnCl_2$ and oxalic acid. As expected, no peaks from the complex are observed in the ^1H NMR spectrum, while the ^{13}C NMR spectrum displays a peak at 160.9 ppm, which falls in the region of carboxylic acids and matches the chemical shift of oxalic acid.[4]

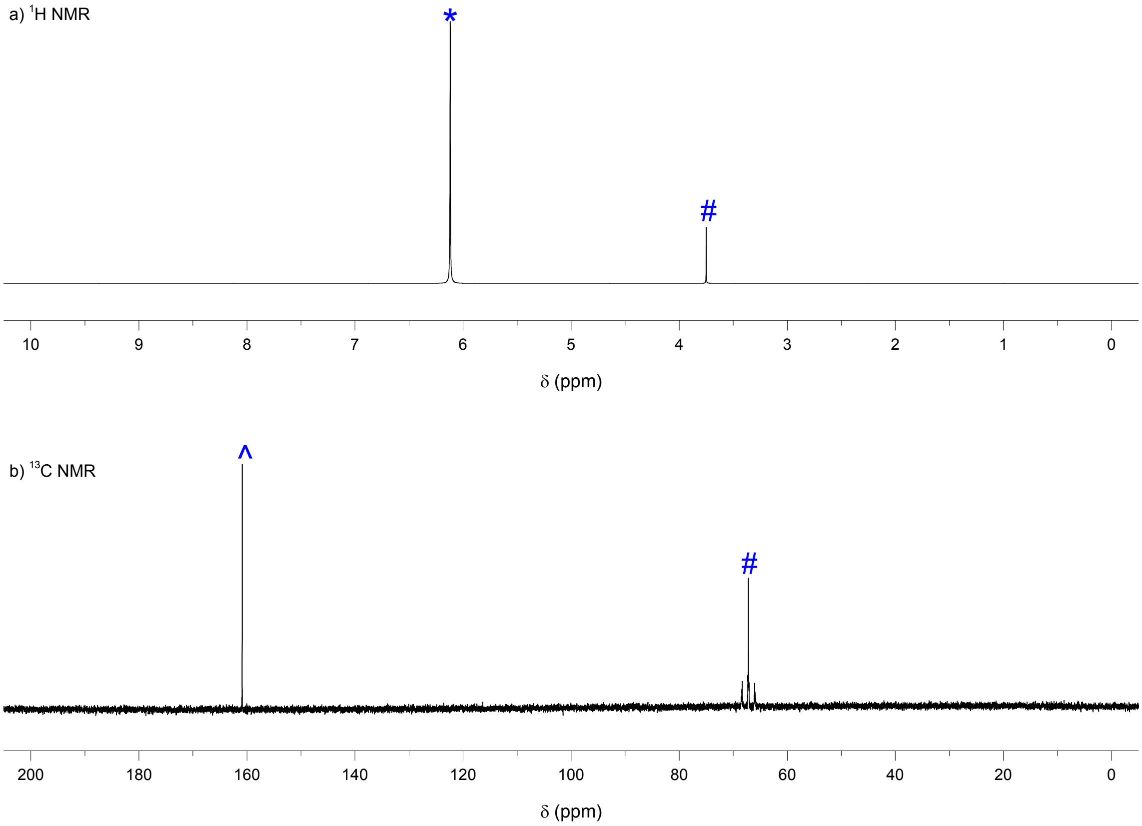

Figure S 3 : NMR Spectra of Zn product. a) ^1H NMR spectrum of Zn product, peak labelled # results from 1, 4-dioxane and peak labelled * results from water. b) ^{13}C NMR spectrum of Zn product, peak labelled # results from the reference 1,4-dioxane with the splitting of the peaks due to with partially deuterated 1,4-dioxane. Peak labelled ^ results from oxalic acid. (400 MHz, 298K, D_2O containing 1,4-dioxane reference and $DCl_{(aq)}$)

Material characterisation of heat-treated samples

Raman and FTIR spectra for as-isolated and F2N matched those of ferrous oxalates previously published [1], and that of F3A was similar to the distinct pattern seen in α-Fe_2O_3.[5, 6] Meanwhile, Raman and FTIR spectra for F3N and F4N (Figure S 4) matched those of γ-Fe_2O_3. Three broad Raman bands below 1000 cm^{-1} for F3N and F4N (I, II, III in Figure S 4a, F3N: at 654, 506, 700, and F4N: 372, 490, 670 – 720 cm^{-1}) occurred at frequencies characteristic of either γ-Fe_2O_3 or Fe_3O_4,[5, 6] with the uncertainty due to possible phase transformations induced by the laser during Raman analysis.[5, 6] Distinction between γ-Fe_2O_3 and Fe_3O_4 was made using features in the 400 – 1000 cm^{-1} region of the FTIR spectra (Figure S 4b). The presence of multiple absorption peaks and shoulders in the region of 750 – 400 cm^{-1} indicated that the samples were γ-Fe_2O_3; with Fe_3O_4 expected to show one peak at 590 cm^{-1}.[7, 8] Rietveld refinement was performed indicated that F4N was c.a. γ-Fe_2O_3 and 15% Fe (Figure S 5).

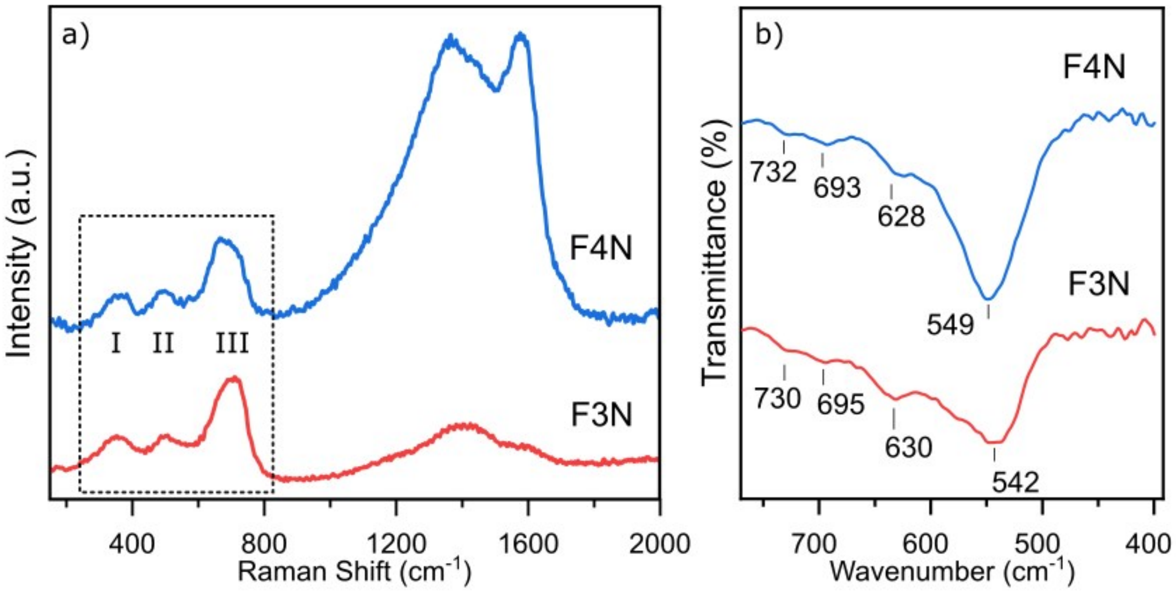

Figure S 4: a) Raman and b) FTIR spectra of F3N and F4N. The combination of FTIR peaks between 750 – 400 cm^{-1} , and the identified Raman peakse (I,II,III) suggests that the samples consist of Fe_2O_3 instead of Fe_3O_4.

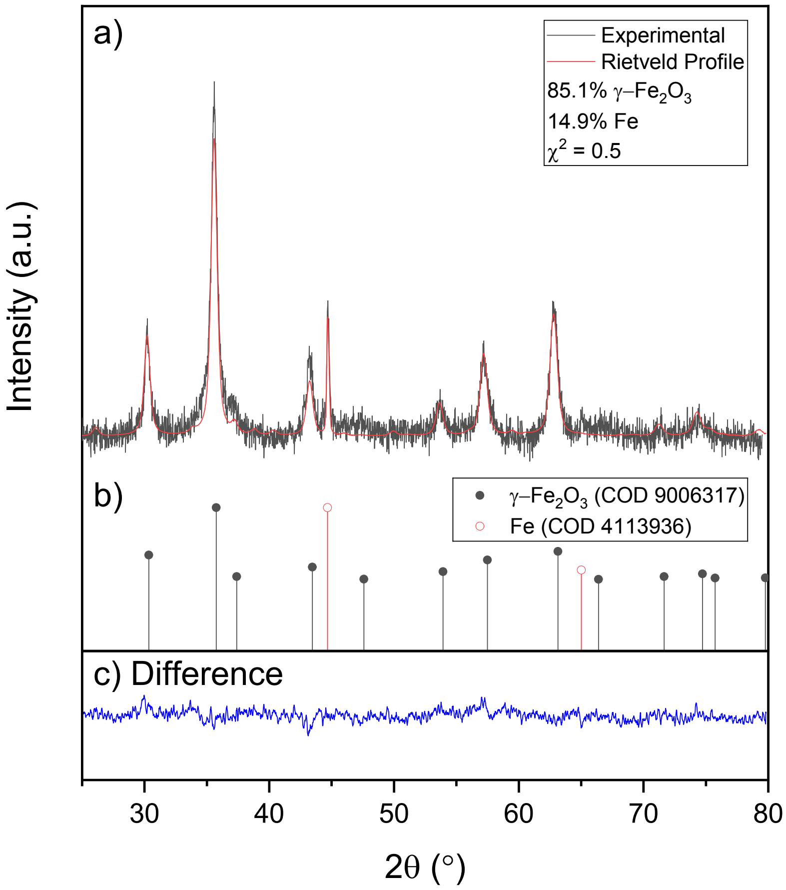

Figure S 5: Phase quantification of F4N using Rietveld refinement; indicating that the sample consisted of c.a. 85.1% γ-Fe_2O_3 and 14.9% Fe. a) Experimental PXRD pattern of and the XRD profile obtained from Reitveld refinement using b) reference patterns for α-Fe (COD 4113936) and γ-Fe_2O_3 (COD 9006316). c) Difference between the Rietveld profile and experimental data.

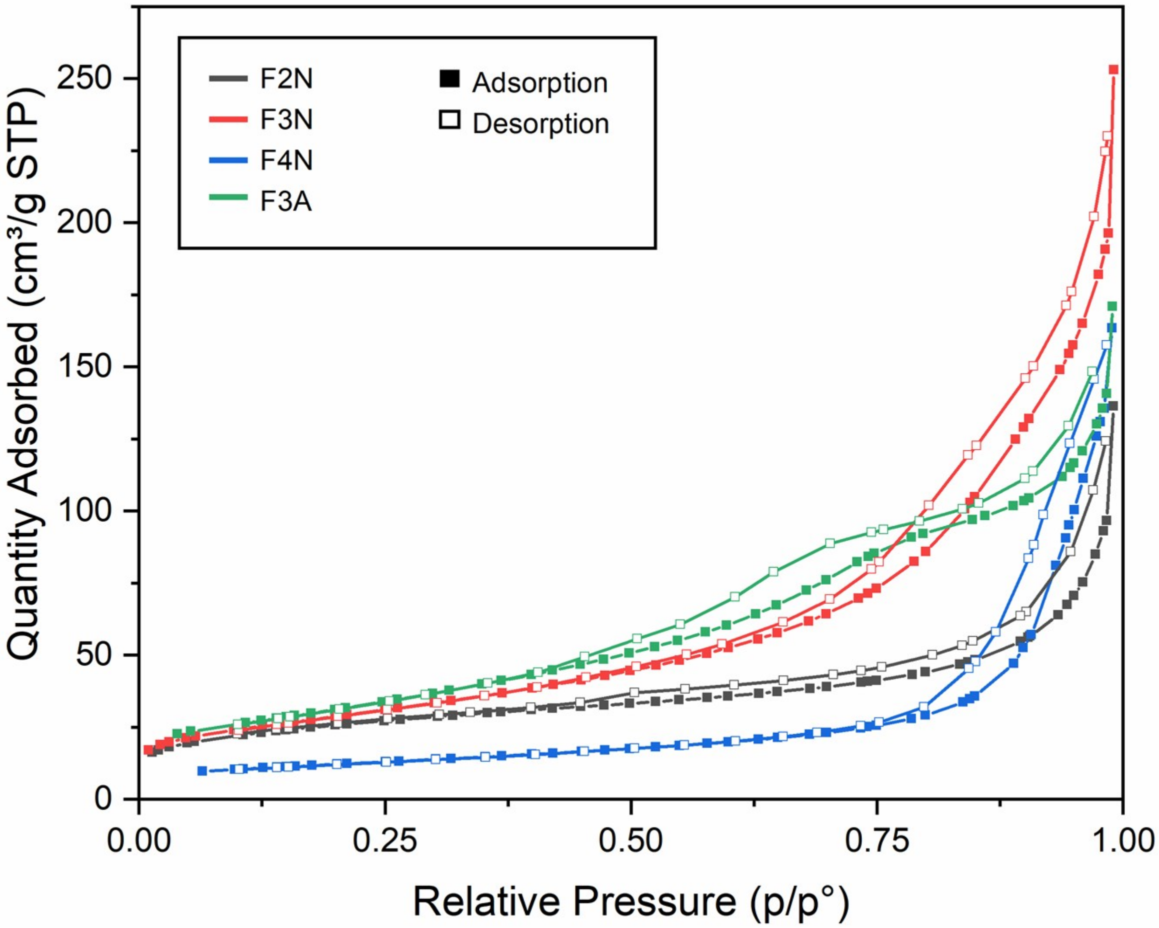

Figure S 6: Adsoprtion and desorption isotherms for F2N, F3N, F4N and F3A

XPS analysis

For XPS analysis the powders were loaded and gently packed on a grooved sample holder before insertion in ultra-high vacuum. The spectra were collected on a Nexsa Surface Analysis System (ThermoFisher) with a monochromated Al KαX-ray gun. While the system is equipped with a flood gun for charge neutralization, the alignment of the spectra was double-checked with the position of the C1s core level for the C-C bond (284.7eV). Survey spectra were collected at a pass-energy 150 eV, core levels at a pass-energy 50 eV. For every sample survey spectra and C1s core levels were collected on 3 different spots, to check the sample homogeneity. Values reported in the main text are the averaged values. XPS analysis was performed via Igor Pro software via the XPST package;[9] all components were fitted with a Voigt lineshape.

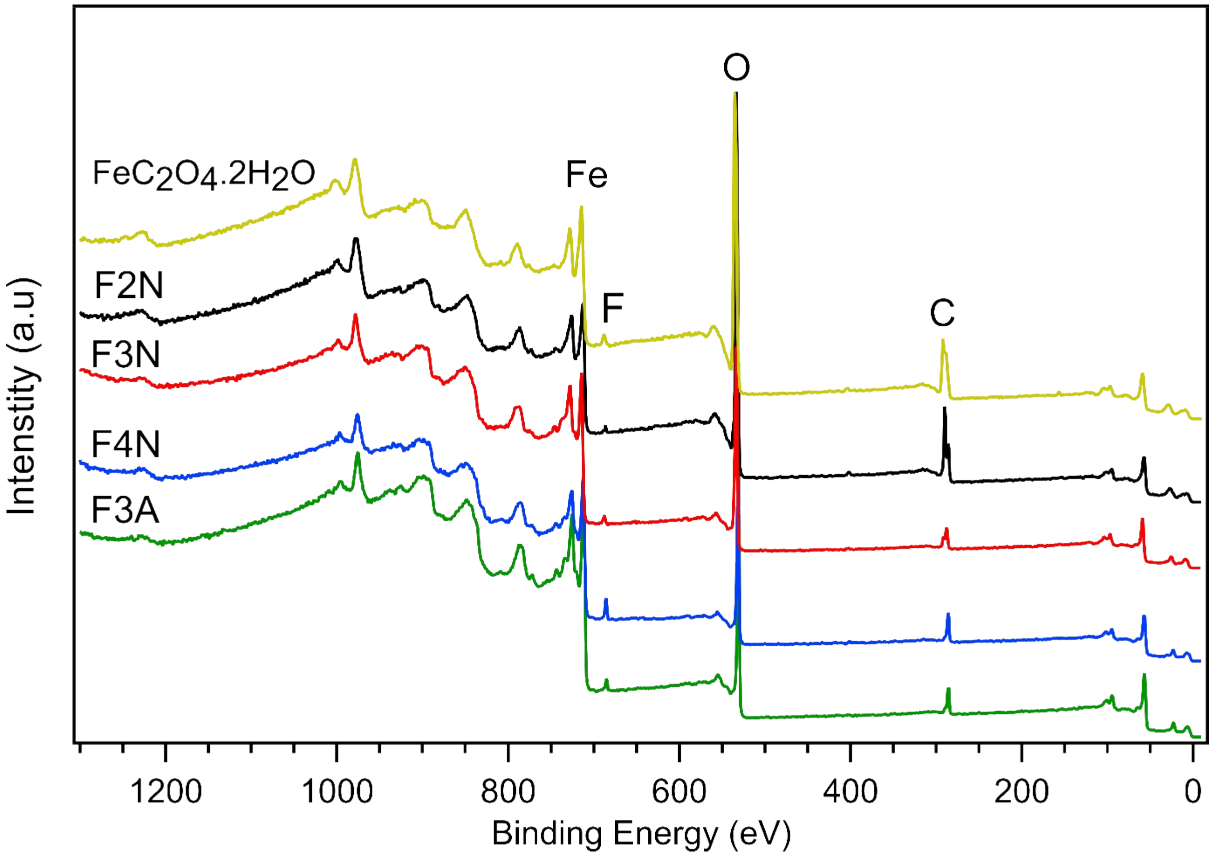

Figure S 7: X-ray Photoelectron Spectroscopy (XPS) survey spectra of $FeC_2O_4.2H_2O$, F2N, F3N, F4N, and F3A, showing the presence of Fe, O and C from FeC_2O_4. Samples contained traces of F, possibly from the electrolyte salt (used during material synthesis, TEA-BF_4). Spectra vertically offset for clarity.

Table S 3: Elemental ID and Quantification of $FeC_2O_4.2H_2O$ using XPS

Name	*Start BE*	*Peak BE*	*End BE*	*Height CPS*	*FWHM eV*	*Area (P) CPS.eV*	*Atomic %*
C1s	295.08	290.10	281.58	34236.60	3.08	179008.07	34.22
F1s	697.08	686.33	676.08	7430.02	2.97	43073.26	2.71
Fe2p	740.08	712.74	701.08	68067.16	5.88	730036.65	13.51
O1s	539.08	533.71	524.08	175213.12	3.00	627833.07	49.56

Table S 4: Elemental ID and Quantification of F2N using XPS

Name	*Start BE*	*Peak BE*	*End BE*	*Height CPS*	*FWHM eV*	*Area (P) CPS.eV*	*Atomic %*
C1s	297.13	289.79	274.88	101752.13	1.76	495123.65	34.35
Fe2p	759.27	712.40	694.35	180397.07	3.72	1953533.22	13.12
O1s	541.07	532.94	514.36	522124.69	2.97	1834354.95	52.53

Table S 5: Elemental ID and Quantification of F3N using XPS

Name	*Start BE*	*Peak BE*	*End BE*	*Height CPS*	*FWHM eV*	*Area (P) CPS.eV*	*Atomic %*
C1s	295.58	286.88	280.58	43981.00	3.29	217617.83	21.04
F1s	693.08	686.33	682.08	18618.00	3.23	78154.02	2.49
Fe2p	742.90	713.01	702.08	268850.99	4.35	2094066.49	19.65
O1s	541.58	532.29	524.08	404224.21	3.23	1422069.03	56.82

Table S 6: Elemental ID and Quantification of F4N using XPS

Name	*Start BE*	*Peak BE*	*End BE*	*Height CPS*	*FWHM eV*	*Area (P) CPS.eV*	*Atomic %*
C1s	298.08	285.92	273.53	49923.24	2.77	192081.24	23.02
F1s	698.08	685.34	676.08	36481.30	2.69	126531.96	5.00
Fe2p	740.08	712.16	698.08	217935.73	4.67	2085139.07	24.25
O1s	540.08	531.18	517.50	295956.77	2.76	963720.25	47.73

Table S 7: Elemental ID and Quantification of F3A using XPS

Name	*Start BE*	*Peak BE*	*End BE*	*Height CPS*	*FWHM eV*	*Area (P) CPS.eV*	*Atomic %*
C1s	296.08	285.47	279.08	60960.34	1.79	247041.15	17.55
F1s	696.08	685.06	678.08	29483.42	3.01	144681.27	3.39
Fe2p	740.08	711.55	701.51	409219.90	2.93	4034534.73	27.79
O1s	540.08	530.50	523.08	513006.99	1.54	1747593.34	51.27

Morphology comparison with literature

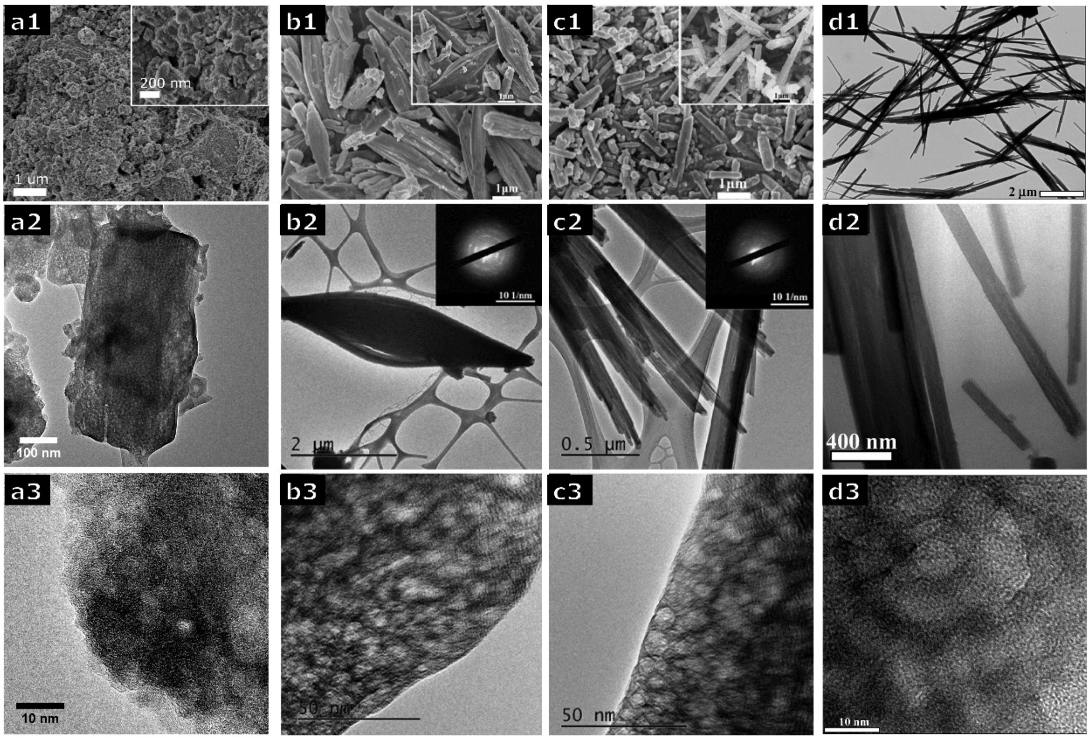

Figure S 8: Comparison of FeC_2O_4 morphology produced in this study (a – F2N) with those produced using (b and c) a *chimie douce* method,[10] and (d) reverse micelles method.[11] SEM and TEM images at lower mgnifications (a1, a2, b1, b2, c1, c2, d1 and d2) show that electrochemical synthesis leads to smaller but more irregular particle size and shapes. Similar porous structures amongst all samples were observed in the TEM images at higher magnifications (a3, b3, c3, and d3). (b1, b2, b3, c1, c2 and c3) Reprinted (adapted) with the permission from Ang *et al.*,[10] Copyright (2012) American Chemical Society. (d1, d2and d3) Reprinted (adapted) with the permission from Aragón *et al.,*[12] Copyright (2008) American Chemical Society.

Table S 8: Comparison of chemicals used when $FeC_2O_4.2H_2O$ is prepared via different synthesis methods; electrochemically (this study), via *chimie douce*[10] and via reverse micelles methods.[13]

Reference	Method	Chemicals consumed
This study	Electrochemical synthesis	200 ml 0.1 M TEA-BF_4 in acetonitrile, CO_2 (unknown quantity), scrap mild steel (unknown quantity), 200 ml H_2O
[10]	*Chimie douce* (Solution 1 mixed with solution 2)	Solution 1: 89 mg of $H_2C_2O_4$, 10 ml of N,N-diethylacetamide (DEAc), 10 ml of N-methyl-2-pyrrolidione (NMP), Solution 2: 198 mg of $FeCl_2 \cdot 4H_2O$, 5 ml of H_2O
[13]	Reverse micelles (Solution 1 mixed with solution 2)	Solution 1: 16.76% cetyl-trimethy-lammonium bromide (CTAB), 13.9% hexanol, 59.29% isooctane, 10.05% 0.3 M aqueous iron(II)sulfate solution Solution 2: 16.76% cetyl-trimethy-lammonium bromide (CTAB), 13.9% hexanol, 59.29% isooctane, 0.3 M aqueous ammonium oxalate

Galvanostatic cycling

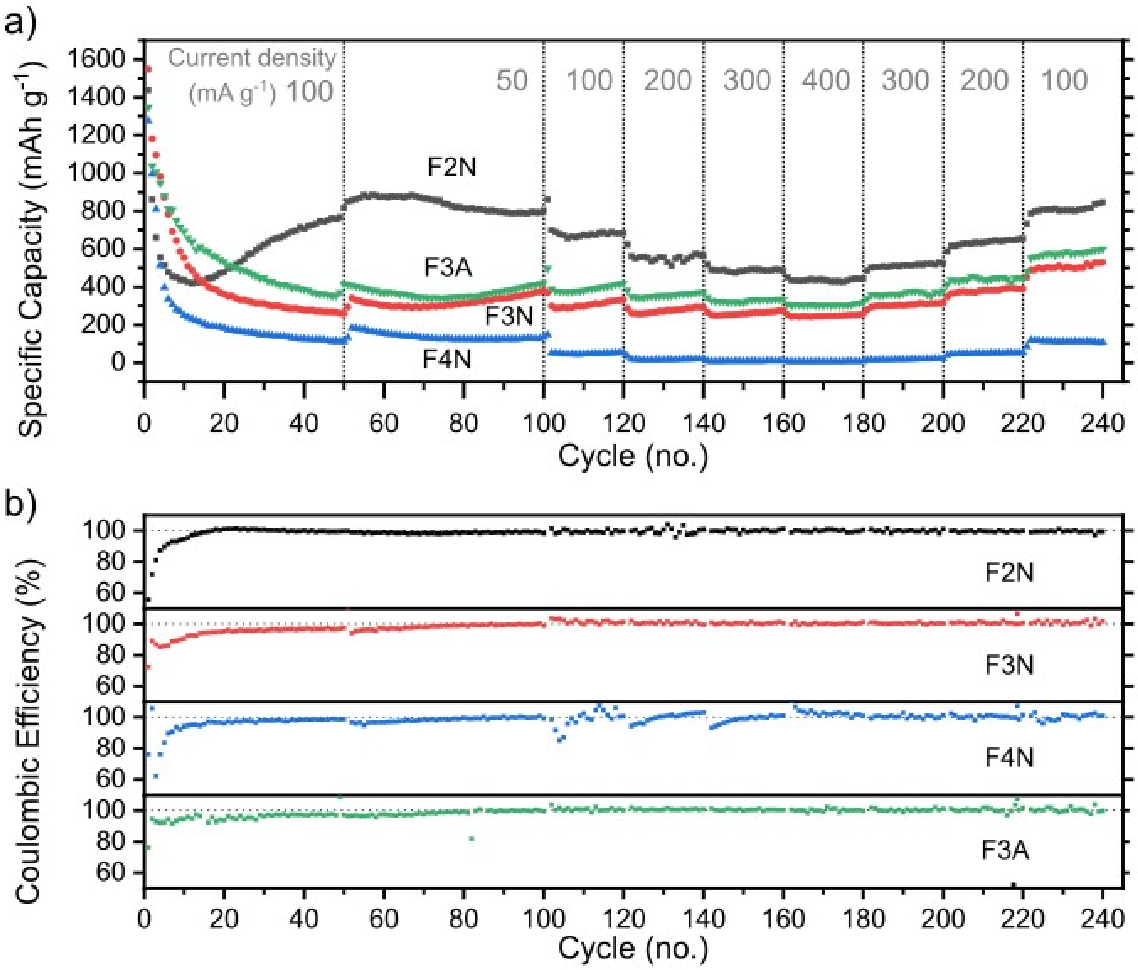

Figure S 9: a) Discharge capacity and b) associated Coulombic efficiency of samples during galvanostatic cycling at variable current densities.

Capacity contributions

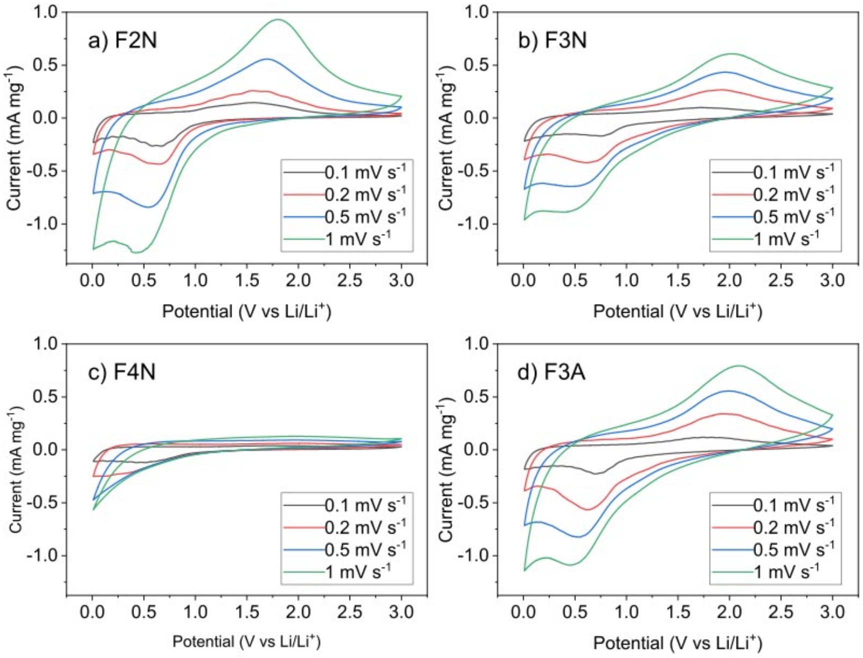

Figure S 10: Cyclic voltammograms of F2N, F3N, F4N and F3A, with sweep rates of 0.1, 0.2, 0.5 and 1 mV s^{-1}.

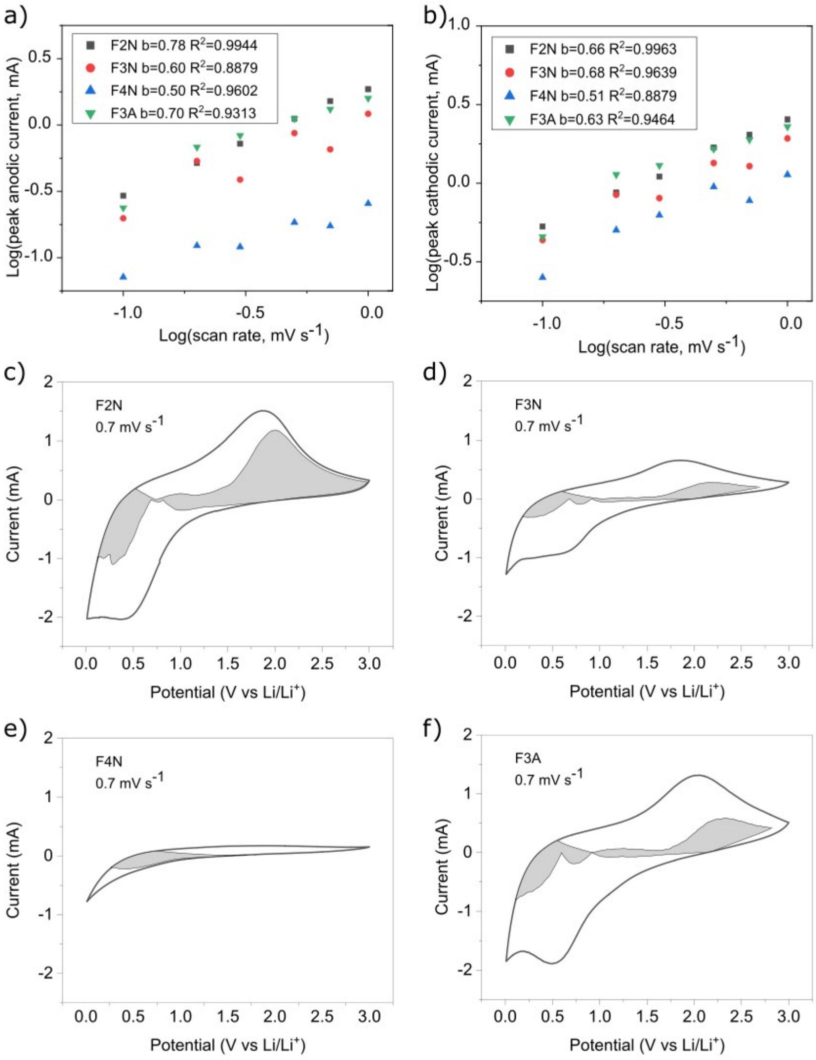

Figure S 11: (a, b) Relationship between the logarithm cathodic/anodic peak current and logarithm scan rates, where b values are provided in the context of $i=av^b$, i = current, v = scan rate, a = constant. (d-f) Capacitive contributions (shaded region) of each sample at 0.7 mV s^{-1}, e) capacitive contribution of each material at different scan rates.

The cathodic/anodic peak currents (i) can be related to the scan rates (v) via Eq. S7.

$$i=av^b \text{ (Eq. S7)}$$

in Eq. S7, *a* and *b* are constants. The value of b can be determined by plotting the values of log(i) with respect to log(v) (see Figure S7 a, b); the gradient of a line of best fit corresponds to the value of *b*. Two well-defined cases occur when *b* is 0.5 or 1; the first indicates only diffusion-based controlled processes, and the latter indicates purely capacitive processes.

The value of *b* for F2N is approximately 0.7, the highest amongst the samples considered, indicating that it is between an ideal capacitor and pure diffusion controlled. In contrast, *b* is close to 0.5 for F4N and F3A, indicating almost entirely diffusion-controlled processes that contribute to the total capacitance. Deviations of from linearity observed in Figure S7 (a,b), particularly at scan rates of 0.3 and 0.7 mV s^{-1} can be attributed to electrode degradation as the electrode was cycled repeatedly; noting that the electrodes were not necessarily cycled in order of increasing sweep rates.

Despite the effects of electrode degradation, the b-value of F2N remained higher than the oxide samples after further CV cycling. Table S3 summarises the b-values obtained after the electrodes were cycled five and 42 times. Values of R^2 are close to one, showing that the linear relationship. b-values outside the range of 0.5 – 1 may also be attributed to changes in the current response associated with material degradation as the electrode is cycled repeatedly.

Table S 9: b-values for oxalate and oxide samples after cycling five and 42 times, calculated based on peak anodic and cathodic current responses observed while cycling at 0.1, 0.2, 0.3, 0.5, 0.7, 1 and 2mV s^{-1}.

CV Cycle number	Material	Anodic		Cathodic	
		b	R^2	b	R^2
5 – 21	F2N (200°C N_2)	0.78	0.9944	0.66	0.9963
	F3N (300°C N_2)	0.68	0.8879	0.60	0.9639
	F4N (400°C N_2)	0.50	0.9602	0.51	0.8879
	F3A (300°C Air)	0.70	0.9313	0.63	0.9464
42 – 57	F2N (200°C N_2)	0.76	0.9865	0.70	0.9841
	F3N (300°C N_2)	0.46	0.9975	0.40	0.9828
	F4N (400°C N_2)	0.36	0.9985	0.11	0.8697
	F3A (300°C Air)	0.43	0.9963	0.43	0.9518

Carbon content calculations

Quantity of as-synthesised material ($M_{S,T}$) required for 1 g of active material was determined using experimental yield (Y_T) from the heat treatment process. Y_T was determined by measuring the mass of as-synthesised material before heat treatment, and the mass of product after heat treatment.

$M_{S,T} = 1\ \mathrm{g} / Y_T$ (Eq. S8)

Y_T = mass before heat treatment/ mass after heat treatment (Eq. S9)

Mass of carbon in 1 g of active material ($M_{A,C}$) and in the required quantity of starting material ($M_{S,C}$) was calculated using the carbon content obtained experimentally through CHN analysis. Where $\%C_{Exp,A}$ is the carbon content of heat-treated materials (F2N, F3N, F4N and F3A), and $\%C_{Exp,S}$ represents the carbon content of the as-synthesised $FeC_2O_4.2H_2O$.

$M_{A,C} = 1\ \mathrm{g} * \%C_{Exp,A}$ (Eq. S10)

$M_{S,C} = M_{S,T} * \%C_{Exp,S}$ (Eq. S11)

The normalisation of the values with respect to discharged capacity was performed by dividing the values by the discharged capacity

Table S 10: Summary of carbon stored and loss per gram of material

Sample	**$M_{A,T}$ [g]**	**$\%C_{Exp}$**	**$M_{S,T}$ [g]**	**$M_{S,C}$ [g]**	**C loss $M_{S,C} - M_{A,C}$ [g]**	**% C loss (C loss)/ $M_{S,C}$**
As-synthesised	1	11.5	1	0.115	0	0
F2N (200°C N_2)	1	12.2	1.29	0.148	0.026	17.8
F3N (300°C N_2)	1	2.1	1.98	0.227	0.206	90.8
F4N (400°C N_2)	1	0.9	2.00	0.231	0.222	96.1
F3A (300°C Air)	1	0.5	2.02	0.232	0.227	97.8

Table S 11: Specific discharge capacity values used for normalising stored carbon

Scenario		F2N	F3N	F4N	F3A
1	lowest value in the last 20 cycles	810	500	110	575
3	50th cycle at 100 mA g^{-1}	767	262	114	356
4	Average at 400 mA g^{-1}	430	245	7	300

The reference value for graphite was calculated based on the theoretical capacity of 372 mAh g^{-1}. 2.67 g of graphite is therefore required for one Ah of energy storage. As the entire material is based on carbon (i.e. Carbon content = 100%), carbon stored for graphite is 2.67 g Ah^{-1}.

Specific capacity comparison with literature

Table S 12: Specific Capacity comparison

Ref.	**Material**	**Synthesis Method**	**Charge/discharge Rate (C = 1 Li h^{-1} mol^{-1})**	**Specific discharge capacity (active material mass) [mAh g^{-1}]**	**Electrode composition** [Active material: conductive additive: polymer Binder (w:w:w)] **and Separator**
This study	FeC_2O_4	CO_2 electrochemical reduction	100 mA g^{-1}	767 (50 cycles) 810 (100 cycles)	80:10:10 Glass fibre
This study	FeC_2O_4	CO_2 electrochemical reduction\	400 mA g^{-1}	430	80:10:10 Glass fibre
[11]	FeC_2O_4	Reverse micelles	2C	433 (74 cycles)	60:30:10 Glass fibre
[12]	FeC_2O_4	Reverse micelles	2C	480 (70 cycles)	60:30:10 Glass fibre
[13]	FeC_2O_4	Reverse micelles	1C	300 (70 cycles)	60:30:10 Glass fibre
[10]	FeC_2O_4	*Chimie douce*	1C	869(50 Cycles) 825(100 cycles)	60:30:10 Celgard 2400 membrane
[10]	FeC_2O_4	*Chimie douce*	1C	739 (50 cycles) 906 (100 cycles)	60:30:10 Celgard 2400 membrane

Supporting information references

1. M. C. D'Antonio, A. Wladimirsky, D. Palacios, L. Coggiolaa, A. C. González-Baró, E. J. Baran and R. C. Mercader, *Journal of the Brazilian Chemical Society*, 2009, **20**, 445-450.
2. W. Lv, R. Zhang, P. Gao, C. Gong and L. Lei, *Journal of Solid State Electrochemistry*, 2013, **17**, 2789-2794.
3. H. E. Gottlieb, V. Kotlyar and A. Nudelman, *The Journal of Organic Chemistry*, 1997, **62**, 7512-7515.
4. H. O. Kalinowski, S. Berger and S. Braun, *Carbon-13 NMR spectroscopy*, John Wiley and Sons,New York, NY, United States, 1988.
5. D. L. A. de Faria, S. Venâncio Silva and M. T. de Oliveira, *Journal of Raman Spectroscopy*, 1997, **28**, 873-878.
6. M. Hanesch, *Geophysical Journal International*, 2009, **177**, 941-948.
7. M. Gotić, G. Koščec and S. Musić, *Journal of Molecular Structure*, 2009, **924-926**, 347-354.
8. A. L. Andrade, D. M. Souza, M. C. Pereira, J. D. Fabris and R. Z. Domingues, *Cerâmica*, 2009, **55**, 420-424.
9. M. Schmid, H.-P. Steinrück and J. M. Gottfried, *Surface and Interface Analysis*, 2014, **46**, 505-511.
10. W. A. Ang, N. Gupta, R. Prasanth and S. Madhavi, *ACS Applied Materials & Interfaces*, 2012, **4**, 7011-7019.
11. M. J. Aragón, B. León, C. Pérez Vicente and J. L. Tirado, *Inorganic Chemistry*, 2008, **47**, 10366-10371.
12. B. León, C. P. Vicente and J. L. Tirado, *Solid State Ionics*, 2012, **225**, 518-521.
13. M. C. López, J. L. Tirado and C. Pérez Vicente, *Journal of Power Sources*, 2013, **227**, 65-71.